Energy Transfer in Unsymmetrical Phenylene Ethynylene Dendrimers

Evrim Atas,[†] Zhonghua Peng,[‡] and Valeria D. Kleiman*[,†]

Department of Chemistry, University of Florida, Gainesville, Florida 32611-7200, and Department of Chemistry, University of Missouri—Kansas City, Kansas City, Missouri 64110

Received: March 22, 2005; In Final Form: June 1, 2005

We have applied the fluorescence upconversion technique to explore the electronic excitation energy transfer in unsymmetrical phenylene ethynylene dendrimers. Steady-state emission spectra show that the energy transfer from the dendrons to the core is highly efficient. Ultrafast time-resolved fluorescence measurements are performed at various excitation wavelengths to explore the possibility of assigning absorption band structures to exciton localizations. We propose a kinetic model to describe the time-resolved data. Independent of the excitation wavelength, a typical rise-time value of 500 fs is measured for the fluorescence in the dendrimer without an energy trap, indicating initial delocalized excitation. While absorption is into delocalized exciton states, emission occurs from localized states. When an energy trap such as perylene is introduced on the dendrimer, varying the excitation wavelength yields different energy-transfer rates, and the excitation energy migrates to the trap through two channels. The interaction energy between the dendrimer backbone and the trap is estimated to be 75 cm^{-1}. This value is small compared to the vibronic bandwidth of the dendrimer, indicating that the monodendrons and the energy trap are weakly coupled.

Introduction

The search for artificial light-harvesters has led to intense studies of conjugated dendritic macromolecules.[1−3] Dendrimers have potential applications in photonic devices due to their highly branched architectures and unique physical properties. With recent advances in synthetic methods[4−6] the size, topology, flexibility, and surface chemistry of dendrimers can be controlled at the molecular level with high precision. Accurate positioning of chromophores at the core, periphery, focal point, or even at each branching point of the dendrimer can now be achieved.[7−9] For photonic applications, the dendritic architecture creates large transition dipoles due to the high number of chromophore units.

Some judiciously designed phenylene ethynylene (PE)-based dendrimers have highly efficient, unidirectional energy-transfer properties.[10,11] Their topology suggests applications as scaffolds for light-harvesting devices. In addition, the large number of chromophore units leads to the formation of excitonic bands. These dendrimers' photophysical properties cannot be understood as simply additive properties associated with molecular orbitals on single chromophore units. In this scenario, it is essential to understand the electronic coupling,[12] exciton formation,[11,13] and energy transfer in detail.

A variety of dendritic architectures have now been synthesized, leading to unique photophysical properties. PE units coupled exclusively through meta or para substitution on a phenyl ring lead to either compact or extended dendrimers.[11] These two families of dendrimers differ in the number of PE units between consecutive branching points. Compact dendrimers have a fixed-length linear unit, while extended dendrimers have a variable number of linear PE units depending on the number of branching points between the unit and the core. Both families of dendrimers have been investigated theoretically[13−16] and experimentally.[10,17,18]

In compact dendrimers, steady-state experiments performed by Moore and co-workers show that the optical excitation is localized on the PE units.[11] The excitonic localization on individual PE units is evident by the monotonic increase in absorption intensity and lack of spectral shift with generation number.[2] The extended series exhibit exciton localization on PE units of increasing length (two-, three-, four-ring), which creates an energy funnel yielding multistep energy transfer.

Mukamel and co-workers have studied compact and extended dendrimers using a Frenkel exciton Hamiltonian.[13] Applying the collective electronic oscillator model, they concluded that the electron−hole pair was confined to the linear segments between branching points. The bound Frenkel excitons are free to migrate throughout the molecule. Depending on the strength of the coupling, the migration leads to coherent or incoherent energy transfer. Absorption spectra calculated from this model are in excellent agreement with experiment.

Using time-correlated single-photon counting, Swallen et al.[19] studied an extended PE dendrimer and found an instrument-limited value of about 10 ps for the energy transfer from the lowest energy chromophore in the backbone to a phenylene ethynylene perylene trap. Subsequent experiments by Kleiman et al. investigated the same extended dendrimer using femtosecond degenerate pump−probe spectroscopy and revealed a stepwise energy transfer from the shorter PE units to the longer PE chains.[17] These experiments indicated that some of the steps in the energy transfer occur on a sub-picosecond time scale.

The novel characteristics of PE dendrimers arise from the electronic properties at the branching points. In both compact and extended dendrimers, meta substitutions on the phenyl rings result in broken π-electron conjugation in the ground electronic state. The situation in the excited state is less clear. A recent study based on a diethynylenephenyl unit with H or phenyl substituents shows dramatic changes in both the emission spectra

* Author to whom correspondence should be addressed. Phone: (352) 392-4656 Fax: (352) 392-0872. E-mail: kleiman@chem.ufl.edu.
[†] University of Florida.
[‡] University of Missouri—Kansas City.

10.1021/jp051488z CCC: $30.25
Published on Web 06/28/2005

SCHEME 1: Chemical Structures of Phenylene Ethynylene Dendrimers: (a) $2G_2$-*m*-OH, (b) $2G_2$-*m*-Per, and (c) 3D Model of the $2G_2$-*m*-Per from a MD Simulation

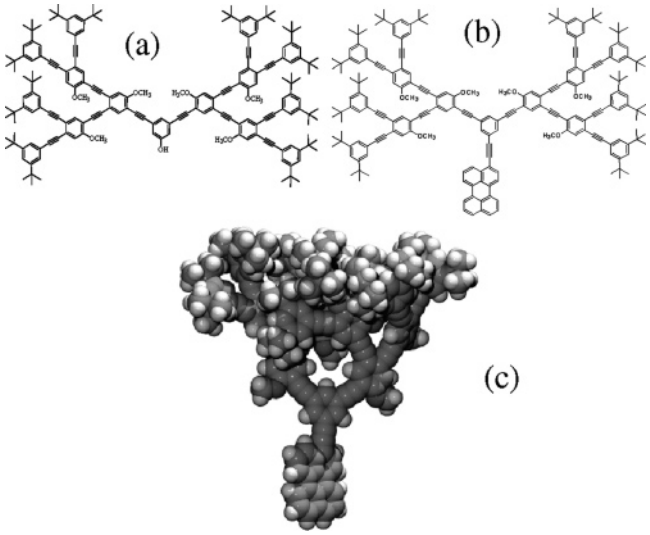

and the radiative lifetimes.[20] The electronic structure calculations indicate that the phenyl ethynylene (H- or phenyl-substituted) units are strongly coupled in a relaxed geometry on the excited state.[12] Experiments in larger dendrimers do not show the shifts predicted in the smaller systems. (See Figure 4 of ref 2.) The extent of localization in the excited state for sizable dendrimers remains an open question.

Unsymmetrical architectures in which coupling among the PE unit occurs through para and ortho substitutions have been synthesized by Peng and co-workers[21−23] (Scheme 1). In these dendrimers, the substitutions create combinations of PE units of variable lengths, analogous to those encountered in extended dendrimers.[21] Unsymmetrical branching leads to rapidly growing conjugation lengths as the generation number increases, providing a broad absorption spectral range with large molar absorptivities and high fluorescent quantum yields.[24] Linear conjugated segments connecting the periphery to the core suggest faster and more efficient energy transfer to the core.[24] Furthermore, the presence of ortho substitutions may allow stronger coupling of PE units, leading to more delocalized excitation throughout the entire molecule. For these architectures, confined Frenkel excitons[13] might extend over regions of the molecule that includes substitutions at ortho positions.

Symmetric dendrimers' absorption spectra can be interpreted as the addition of building blocks, defined by the confined excitons.[13] The role of ortho substitution and exciton confinement in unsymmetric dendrimers is not as well characterized, and there are still unanswered questions: Are the absorption band structures associated with exciton localization and "building blocks"? Does coherent or incoherent energy transfer occur between those localized states?

The goal of our study is to understand the exciton size and the rates of energy migration. We focus here on the characterization of intramolecular interactions and the energy-transfer mechanisms in unsymmetrical PE dendritic molecules. To investigate the extent of delocalization within the dendritic structure, we consider unsymmetrical monodendrons with multiple ortho and para substitutions. Energy-transfer mechanisms are monitored by adding an ethynylene perylene trap (EPer), which acts as reporter for energy transfer.

Time-resolved photoluminescence experiments in the subpicosecond time scale are employed to follow the energy initially deposited in the dendrimer's backbone by an ultrafast pulse. A kinetic model is proposed to interpret the rise times of the fluorescence measured in unsymmetrical dendritic structures with and without an energy trap. Finally, we present an analysis of the validity of the Förster model by comparing the model predictions with our experimental results.

Experimental Section

The synthesis of unsymmetrical PE dendrons has been described elsewhere.[21] Unsymmetrical monodendrons can be combined into larger structures, leading to more symmetric macromolecules. For example, Scheme 1a shows two G_2 (generation 2) dendrons coupled to a phenyl ring in the meta positions. The phenyl ring has an additional OH group in the other meta position and is thus named $2G_2$-*m*-OH. The addition of an energy trap to a similar structure can be used to quantitatively probe the energy-transfer dynamics. In this case, an ethynylene perylene unit replaces the OH group, leading to the $2G_2$-*m*-Per molecule as shown in Scheme 1b. Even though the chemical structure seems to describe a planar molecule, the three-dimensional (3D) modeling shown in Scheme 1c clearly demonstrates otherwise. To obtain a reasonable picture of the room-temperature structure of $2G_2$-*m*-Per, we look at a molecular dynamics (MD) simulation performed by Roitberg and Krause.[25] After several nanoseconds of the MD run, a snapshot (Scheme 1c) was taken showing the globular shape of the dendrimer. The small size of this dendrimer and its rigidity do not allow for the "fold-back" of any of the branches. In addition, the trap is completely exposed, with the dendritic structure forming a sort of "bouquet".

Steady-state characterization of the didendrons is performed via UV−vis absorption in a Varian-Cary 100 and emission in a Jobin-Yvon instrument (Spex Fluorolog-3). All steady-state measurements are performed in the same home-made rotating cell (optical path of 1 mm), which is also used for the time-resolved experiments. Sample concentrations are kept below 10^{-6} M to avoid any aggregation[26] or excimer formation,[27] yielding optical densities less than 0.3 mm^{-1}. Femtosecond time-resolved photoluminescence is employed to explore excited-state dynamics and energy transfer. The upconversion experiment measures the temporal evolution of the fluorescence with sub-picosecond resolution. It is based on the sum-frequency mixing of the molecules' emission with an ultrafast gate pulse in a nonlinear crystal (Figure 1). Excitation pulses are derived from an optical parametric amplifier (OPA), pumped by a commercial Ti−sapphire laser system consisting of a Ti−sapphire oscillator (Tsunami, Spectra-Physics) and subsequent amplifier (Spitfire, Spectra-Physics) with a repetition rate of 1 kHz. The fourth harmonic of the OPA output signal or idler is used to generate tunable excitation pulses in the 320−470 nm spectral region. Pump pulses of ∼40 nJ with a beam diameter of 200 μm are used to maintain a linear optical response.

After all the optics in the OPA and harmonic generation processes, the UV and visible pulses accumulate group velocity dispersion, yielding longer excitation pulses and poor experimental time resolution. To overcome this pulse lengthening, we use a pair of quartz prisms to compensate for the chirp. The instrument response function (IRF) is measured with pump scattered light, which is upconverted with the gate pulse yielding cross correlations full width at half-maximum (fwhm) of 175 and 220 fs in the visible and UV regions, respectively. Data analysis involves the convolution of decay and rise-time functions with the corresponding experimental IRF.

The home-made rotating cell has a 1 in. diameter and an optical path length of 1 mm to guarantee excitation of a new

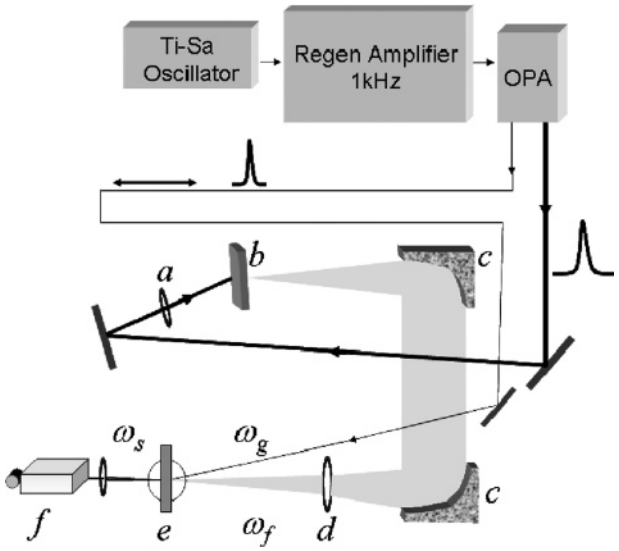

Figure 1. Fluorescence upconversion setup: a, focusing lens (200 mm) for excitation beam; b, sample (rotating holder); c, off-axis parabolic mirrors (effective focal length 152 mm); d, concave lens (−200 mm) for fluorescence magnification; e, β-BBO crystal, type I (0.5 mm); f, 0.25 m monochromator and PMT; ω_g, gate frequency; ω_f, fluorescence frequency; $\omega_s = \omega_g + \omega_f$, signal frequency.

sample volume with every laser shot with minimum consumption of sample. The photoluminescence is collected by two off-axis parabolic mirrors (effective focal length = 152 mm), and the excitation volume is imaged onto a 500 μm β-barium borate (β-BBO) crystal.

A small portion of the regenerative amplifier beam (~30 μJ/pulse, fwhm = 60 fs) is weakly focused (50 cm focal length), and the beam diameter at the crystal is kept larger than the imaged fluorescence. Spatially and temporally overlapped gate and collected fluorescence in the β-BBO crystal generates a nonlinear response signal in the UV. Colored filters (UG11) are used to remove scattered light from the excitation pulse and the second harmonic of the gate, which is also generated at the crystal. The upconverted beam is dispersed by a 0.25 m monochromator and detected with a photomultiplier tube (PMT). Boxcar integration and averaging of 10^4 pulses leads to a signal-to-noise ratio of about 50:1

The photostability of the sample is checked by steady-state UV and emission spectroscopy before and after each time-resolved experiment.[28]

Results

Steady-State Spectroscopy of Phenylene Ethynylene Dendrimers. G_2-OH is a second-generation unsymmetrical (PE) dendron; $2G_2$-*m*-OH is a didendron consisting of two G_2 dendrons coupled through the meta positions of a phenyl ring (Scheme 1a). It has been shown previously that the choice of site substitution on the focal point governs the nature of the optical excitations for the entire molecule.[13,29,30] For the two molecules under consideration ($2G_2$-*m*-OH and $2G_2$-*m*-Per), substitution at the focal point is the same, leading to similar steady-state characteristics as shown in Figure 3. The absorption spectra of $2G_2$-*m*-OH shows a 15 nm red shift compared to the single G_2-OH dendron.[31] This shift is due to the additional phenyl ethynylene unit, which increases the conjugation length in each individual dendron. A better comparison can be made with the steady-state spectra of a generation 3 monodendron (Figure 2). In the G_3OH monodendron, the longest linear PE chain has the same number of PE units as the longest linear

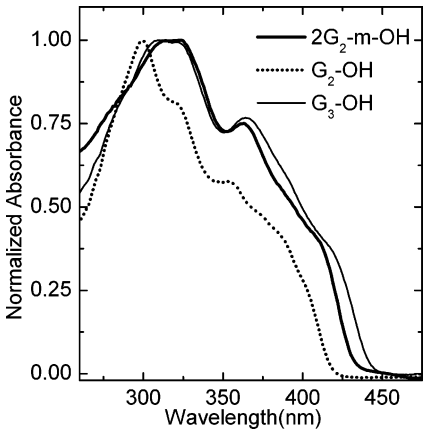

Figure 2. Normalized absorption spectra of $2G_2$-*m*-OH, G_2-OH, and G_3-OH in dichloromethane.

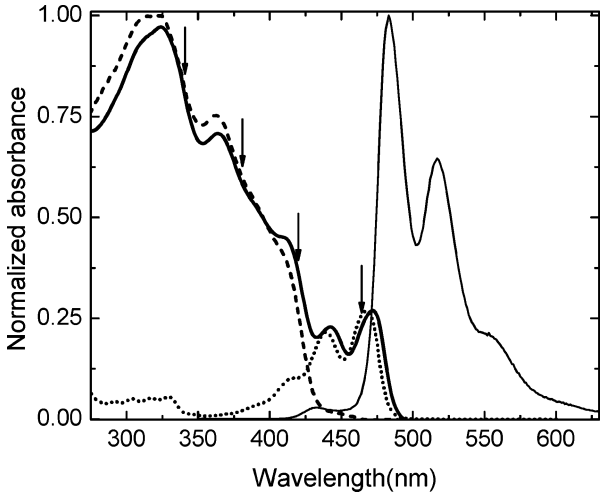

Figure 3. Normalized absorption spectra of (- - -) $2G_2$-*m*-OH, (···) EPer, and (—) $2G_2$-*m*-Per and fluorescence spectrum of (—) $2G_2$-*m*-Per, excited at 320 nm. The arrows indicate the excitation wavelengths used in the time-resolved fluorescence experiments.

chain in the $2G_2$-*m*-OH, and their absorption spectra show similar features (bands, bandwidth, and red shift). There is a slight red shift of G_3OH over $2G_2$-*m*-OH due to some extended conjugation between the two longest linear PE units through the ortho linkage.

To probe the dynamics of energy transfer, EPer is added to the didendron molecule in the meta position with respect to both monodendron components. The absorption spectrum of $2G_2$-*m*-Per resembles the sum of the absorption spectra of $2G_2$-*m*-OH and EPer obtained independently as shown in Figure 3. This suggests a weak ground-state coupling between the dendritic backbone and the EPer energy acceptor. From these spectra, we conclude that the broad absorption feature between 300 and 430 nm corresponds to the dendritic backbone, and absorption at $\lambda > 430$ nm corresponds to direct excitation of the EPer trap. The photoluminescence spectrum shows emission from $2G_2$-*m*-Per originating almost entirely from the EPer trap. At excitation wavelengths between 300 and 400 nm, there is no direct excitation of EPer, and the emission is solely due to energy transfer from the backbone to the trap. This was proven by exciting 2-phenyl ethynylene perylene in CH_2Cl_2 at selected wavelengths and obtaining no emission at 485 nm (maximum wavelength emission). We conclude that energy transfer from the backbone to the trap is very efficient. Comparison of absorption and excitation spectra indicates ~94% efficiency for the energy-transfer process.[21] Interestingly, at 435 nm, we notice

TABLE 1: Lifetime Measurements from TCSPC

	$\lambda_{excitation}$ (nm)	$\lambda_{detection}$ (nm)	τ [a] (ns)
EPer	450	500	2.36 ± 0.01
$2G_2$-*m*-OH	370	450	1.83 ± 0.01
$2G_2$-*m*-Per[b]	370	450	1.83 (52%)
			2.34 (48%)
$2G_2$-*m*-Per	370	500	2.34 ± 0.01

[a] Errors correspond to $\pm 2\sigma$. [b] The τ values were fixed, and only the relative contributions were fitted.

a small band with intensity contributions from incomplete substitution [32] of the OH group in $2G_2$-*m*-OH[21] by EPer and residual backbone emission from $2G_2$-*m*-Per. Time-resolved data will clarify the origin of this backbone fluorescence band.

Time-Resolved Emission Experiments. The fluorescence decays of $2G_2$-*m*-OH and $2G_2$-*m*-Per occur on a nanosecond time scale and are measured by time-correlated single-photon counting (TCSPC). The fluorescence decays for these dendrimers are characterized by a single-exponential decay (Table 1). The decay for the $2G_2$-*m*-Per at 500 nm is in very good agreement with that of the 2-phenyl ethynylene perylene emission lifetime at the same wavelength. Detection of $2G_2$-*m*-Per emission at 450 nm yields a combination of the emission lifetime of $2G_2$-*m*-Per (measured at 500 nm) and unsubstituted $2G_2$-*m*-OH, whose fluorescence spectrum has a peak at 450 nm.

The rise times associated with these fluorescence decays were measured by the femtosecond time-resolved fluorescence upconversion technique. To understand the excitation delocalization and intramolecular interactions within the didendron backbone, we first study the dynamics in the absence of the EPer trap.

The absorption spectrum of $2G_2$-*m*-OH has three distinguishable bands peaked at 320, 363, and 411 nm. Exciting $2G_2$-*m*-OH at selective wavelengths (330, 372, and 415 nm), we seek to probe regions with considerable contributions from each band and explore the possibility of assigning the absorption band structure to exciton localization.

After excitation at the selected wavelengths, emission is detected at 435 nm corresponding to backbone fluorescence (Figure 4). Convolution of the instrument response function and the exponential rise function (see model below) reveals a 500 fs time constant. It is important to note that the fitting involves the convolution of the IRF with the model functions, and therefore the experimental time resolution is ca. 150 fs (slightly better than the IRF fwhm). The surprising result is the lack of rise-time dependence on excitation wavelengths. The three plots in Figure 4 show similar rise times (510 ± 20 fs at $\lambda = 330$ nm, 540 ± 30 fs at $\lambda = 372$ nm, and 500 ± 35 fs at $\lambda = 420$ nm). We conclude that the initially excited state must be delocalized throughout the monodendron, and it takes about 500 fs to reach the lowest-lying state (the emissive state).

As mentioned previously, when the EPer trap is attached to the didendron, a strong emission from the EPer unit is observed, which indicates efficient energy transfer. To follow the energy migration from the initially excited state on the didendron backbone to the EPer trap, we measure the rise time of the EPer emission. Figure 5 shows the temporal evolution of the $2G_2$-*m*-Per fluorescence as a function of excitation wavelengths. The fits correspond to the convolutions of exponential functions (see kinetic model below) with the instrument response function. The excitation wavelengths are shown as arrows in the absorption spectrum in Figure 3. Detection of the fluorescence is at the EPer maximum emission wavelength ($\lambda = 485$ nm). Part a in Figure 5 shows the emission response following direct excitation of the EPer trap at 465 nm. A single-exponential

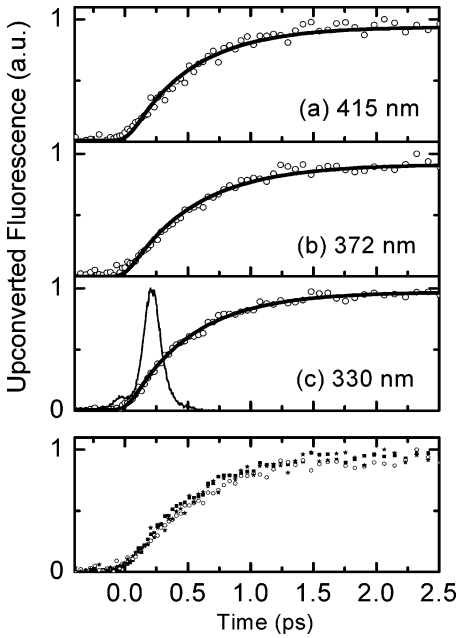

Figure 4. $2G_2$-*m*-OH in dichloromethane excited at (a) 415 nm, (b) 372 nm, and (c) 330 nm. Upconversion signal of fluorescence is detected at 435 nm, the maximum emission wavelength of the molecule. Fitting procedures include the convolution of exponential functions from the kinetic model with the IRF. The best fit is shown as the solid line. The longest IRF function is shown in part c. The bottom panel shows the superposition of the experimental data in parts a−c.

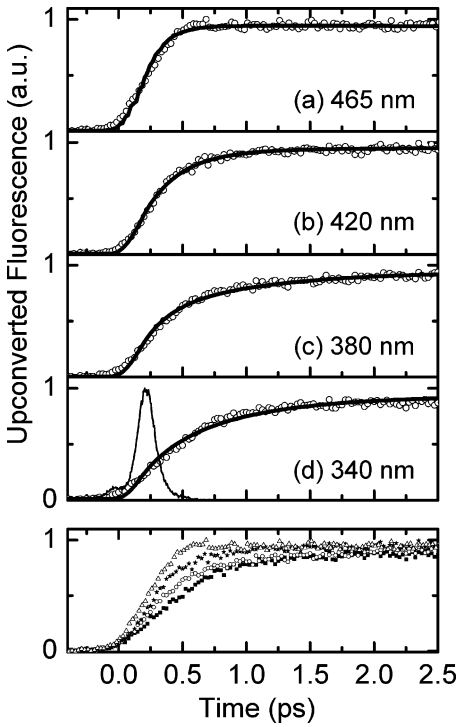

Figure 5. Upconversion signal of $2G_2$-*m*-Per in dichloromethane, excited at (a) 465 nm, (b) 420 nm, (c) 380 nm, and (d) 340 nm. Fluorescence signal is detected at 485 nm, the maximum emission wavelength of the $2G_2$-*m*-Per molecule. The fittings correspond to the convolution of the IRF and the decays shown in Table 2. The longest IRF function (at 340 nm) is shown in part d. The bottom panel shows the superposition of the experimental data in parts a−d.

function ($\tau \approx 150$ fs) yields a good fit to the experimental data, which provides the time-resolution limit for fluorescence rise times. Any rise time longer than that limit can therefore be attributed to excited-state dynamics in the backbone and energy

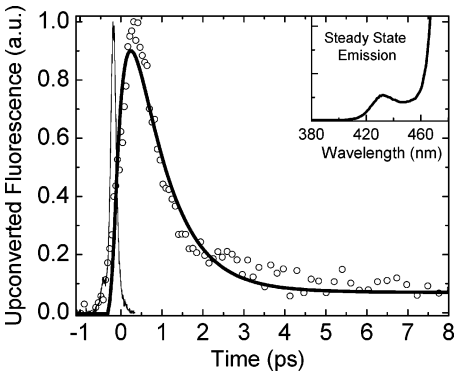

Figure 6. Upconversion signal of $2G_2$-*m*-Per: $\lambda_{excitation} = 320$ nm; $\lambda_{emission} = 435$ nm. Solid line is a simulation of the E* fluorescence (equation 4) with fixed time constants from Table 2. Inset shows the steady-state emission spectrum in the region of upconversion detection. See text for details.

transfer to the EPer trap. Part b shows excitation at $\lambda = 420$ nm. At this excitation wavelength, in addition to backbone absorption, there is some residual absorption from the EPer unit. Indeed, there are two mechanisms for the excitation of the EPer acceptor at 420 nm: (i) absorption by the EPer moiety and (ii) sensitized excitation via energy transfer from the backbone. To characterize these two components, we measure the photoluminescence dynamics of a solution containing only EPer in CH_2Cl_2 after direct excitation at $\lambda = 420$ nm. The difference in fluorescence dynamics of $2G_2$-*m*-Per and EPer can be attributed to the backbone-to-EPer energy transfer. After considering the direct excitation component, we still find that the energy absorbed by the didendron backbone is efficiently transferred to the EPer. This component leads to slower dynamics observed after excitation at 420 nm (part b) compared to excitation at 465 nm (part a).

At shorter excitation wavelengths, the fluorescence rise times become even longer. Excitations at $\lambda = 380$ nm (panel c) and $\lambda = 340$ nm (panel d) clearly show longer rise times for the fluorescence arising from the EPer excited state. The longer rise times correspond to energy transfer since at these excitation wavelengths only backbone absorption is observed, and $2G_2$-*m*-OH does not display any long rise times at high-energy excitation wavelengths (Figure 4).

The steady-state fluorescence spectrum (Figure 3) shows that most of the $2G_2$-*m*-Per emission (99%)) derives from the EPer trap. On the blue end of the emission spectrum, a small band is centered at 435 nm, which is the same wavelength as the emission from $2G_2$-*m*-OH. This band has a contribution from the unsubstituted $2G_2$-*m*-OH (as an impurity) and an additional contribution from the backbone emission, even in the presence of the trap. This assertion can be confirmed by examining the time-resolved data detected at $\lambda = 435$ nm (Figure 6). The temporal behavior of the fluorescence shows a very fast rise time followed by a fast decay corresponding to energy transfer from the backbone to the EPer trap. This decay time reflects the average lifetime of the excitation energy deposited in the lowest-lying state of the donor backbone. The long time component (ns) seen in Figure 6 corresponds to unsubstituted $2G_2$-*m*-OH (ref 29). Using the kinetic model described below, we simulate this signal using the time constants obtained from Figures 4 and 5 (including a nanosecond component corresponding to $2G_2$-*m*-OH emission lifetime). Integrating the time-resolved data yields the relative contributions to the steady-state spectrum from the $2G_2$-*m*-OH impurity and the residual backbone emission.

Unsubstituted $2G_2$-*m*-OH emission accounts for more than 99% of the steady-state intensity at 435 nm (corresponding to an impurity concentration of ~1%).[32] The fast decaying component corresponds to less than 1% of the steady-state fluorescence; it can only be detected in the ultrafast time-resolved experiment because of its very fast decaying time.

Discussion

Kinetic Model for Energy Transfer. Both steady-state and time-resolved experiments suggest that the energy-transfer efficiency from the dendrons to the trap is nearly unity. To understand the mechanism of this process and the effect of the electronic structure of the backbone, we must estimate the rate of energy transfer for each individual step. In this section, we propose a model to understand that process through an interpretation of our time-resolved emission data.

We consider the simplest case in which D is the ground state of the backbone, D* is the initially excited state, and E* is the emissive state of the backbone.

$$D \xrightarrow{h\nu} D^* \xrightarrow{k_1} E^* \quad (E^* \downarrow k_{rad_{BB}}) \tag{1}$$

According to this model, the 500 ± 40 fs (k_1^{-1}) rise time measured from 2G2-*m*-OH must be attributed to one of the two possibilities, either the emissive state of the backbone is different from the state that is excited initially or the initially excited state undergoes a conformational rearrangement before emitting. The insensitivity of the rise time to pump wavelength indicates delocalization of the optical excitation within the backbone prior to relaxation.

Meta substitution prevents the exciton from delocalizing between the backbone and the EPer unit.[13] Since the meta substitution in the core ring breaks the π-conjugation, we consider that the delocalization occurs within each monodendron.

The addition of the EPer trap results in a new final excited state P*. Emission from the $2G_2$-*m*-Per arises from the P* and the backbone state E*, depending on detection wavelength. This leads to two possible deactivation pathways for the initially excited state, direct

$$D \xrightarrow{h\nu} D^* \xrightarrow{k_3} P^* \quad (P^* \downarrow k_{rad_{BB}}) \tag{2}$$

or indirect

$$D \xrightarrow{h\nu} D^* \xrightarrow{k_1} E^* \xrightarrow{k_2} P^* \quad (E^* \downarrow k_{rad_{BB}};\ P^* \downarrow k_{rad_{Eper}}) \tag{3}$$

Measurements of the $2G_2$-*m*-OH fluorescence probe the E* state directly, whereas experiments with the $2G_2$-*m*-Per probe the EPer emission (P*) when detection is at $\lambda = 485$ nm or backbone emission (E*) from $2G_2$-*m*-Per for early-time detection at $\lambda = 435$ nm.

By solving the kinetic system of equations, we can obtain the population of each excited state with only two free parameters (k_2 and k_3 are free, while k_1 is defined by the fitting to data in Figure 4) in the fitting function. The backbone excited-state population is given by

$$E^*(t) = \frac{k_1}{k_2 - (k_1 + k_3)}[e^{-(k_1+k_3)t} - e^{-k_2 t}] \tag{4}$$

TABLE 2: Fits for Time-Resolved Fluorescence Data

$\lambda_{excitation}$ (nm)	τ_1[a,b] (fs)	τ_2 (fs)	τ_3 (fs)	direct %	indirect %
340	510 ± 20	755 ± 60	440 ± 45	54	46
380	540 ± 30	855 ± 60	305 ± 20	64	36
420	500 ± 35	550 ± 150			
465	150 ± 20				

[a] Time constants (τ_1) for E* and P* are obtained from the time-resolved fluorescence measurement of $2G_2$-*m*-OH and kept constant when fitting the $2G_2$-*m*-Per data. [b] Errors correspond to $\pm 2\sigma$.

The population of the trap excited state (P*) includes two components, indirect (energy goes through the E* state)

$$P_I^*(t) = \frac{k_1 k_2}{(k_2 - k_1 - k_3)}\left\{\frac{-e^{-(k_1+k_3)t}}{k_1 + k_3} + \frac{e^{-k_2 t}}{k_2}\right\} + \frac{k_1}{k_1 + k_3} \quad (5)$$

with $(k_1 + k_3)^{-1}$ and $(k_2)^{-1}$ as characteristic times, and direct

$$P_D^*(t) = \frac{-k_3}{k_1 + k_3} e^{-(k_1+k_3)t} + \frac{k_3}{k_1 + k_3} \quad (6)$$

with $(k_1 + k_3)^{-1}$ as the characteristic time.

The fluorescence lifetimes of E* and P* are on the order of nanoseconds (Table 1), appearing only as a constant offset in the model. The preexponential factors are defined in terms of the rates (eqs 5 and 6), and the relative amplitudes of the contributions for each transfer channel are given by k_1 and k_3. The results are shown in Table 2.

To fit the data for different excitation wavelengths, we consider the relative contribution to the absorption from the EPer unit and/or backbone at, for example, $\lambda = 420$ nm. Allowing this relative contribution to become a free fitting parameter, we obtain from the time-resolved data ~70% contribution from straight excitation of EPer and only ~30% contribution from the excitation via energy transfer from backbone dendrons.

Excitation at 340 and 380 nm (parts d and c in Figure 5, respectively) shows different dynamics with longer rise times. At these wavelengths, there is no direct excitation of EPer, and the emission is solely due to energy transfer from the backbone to the trap through both direct and indirect paths. This was proven by exciting 2-phenyl ethynylene perylene in CH_2Cl_2 at the selected wavelengths and obtaining no emission at 485 nm. Excitation at 340 nm yields the one-step energy transfer (Dir) from the initially excited state with $k_3^{-1} = (440 \pm 45)$ fs and the indirect energy transfer (Ind) (two steps) with $\tau_1 = (510 \pm 20)$ fs (determined from the 2G2-*m*-OH data) and $\tau_2 = (755 \pm 60)$ fs (τ_2). The relative contribution from each path can be evaluated as

$$\text{Ind} = \frac{k_1}{k_1 + k_3} \quad \text{and} \quad \text{Dir} = \frac{k_3}{k_1 + k_3} \quad (7)$$

The results of this procedure suggest that 54% of energy accepted by the EPer is attributed to the direct path, while the contribution from the indirect, multistep pathway is 46%.

At 380 nm, the fit yields a faster rate for the direct path, $\tau_3 = (305 \pm 20)$ fs. At this pump wavelength, the contributions from the direct and indirect channel are 64% and 36%, respectively. As the initially excited state becomes closer to resonance with the EPer transition, the contribution from the direct energy-transfer pathway is more pronounced. This kinetic model reveals that for the indirect channel the slowest step is the energy transfer from the relaxed excited state of the donor (E*) to the acceptor (P*).

A confirmation of the presence of the indirect channel is shown in Figure 6. This figure presents the data collected at 435 nm, a frequency at which there is residual emission from the backbone. In this case, the fast rise and decay times of the fluorescence can be simulated using fixed values of τ_1 (from Figure 4) and τ_2 and τ_3 (from Figure 5, including a nanosecond component corresponding to the $2G_2$-*m*-OH emission lifetime). The agreement between simulation and data is excellent. The rise of the signal is due to $(\tau_1^{-1} + \tau_3^{-1})$, and its decay is given by τ_2; thus it is the energy-transfer process to the acceptor EPer that controls the fast decay of donor fluorescence.

Comparison of absorption with the photoluminescence excitation spectrum indicates that the efficiency of energy transfer for the molecule investigated here is close to unity. The uncertainties associated with measuring excitation spectra when the energy-transfer yields are near unity lead to inaccurate results for the yields. A better approach to measure them is to use time-resolved data. We compare the energy-transfer rate (in this case from the experimental rise time in the acceptor k_{ET}^{-1}) with the donor's fluorescence lifetime in the absence of the acceptor (τ_o) using

$$\phi_{ET} = \left[1 + \frac{1}{k_{ET}\tau_o}\right]^{-1} \quad (8)$$

where ϕ_{ET} is the energy-transfer quantum yield. Considering $2G_2$-*m*-OH as the donor and the EPer as the acceptor, we obtain a $\phi_{ET} > 0.99$, which is in reasonable agreement with the ~0.94 obtained from steady-state measurements.

Energy Transfer in the Weak-Coupling Limit. Mukamel and co-workers' calculations using the Frenkel exciton model[13] assume that meta substitution confines the electron−hole pair (exciton). The possibility of evaluating the coherent coupling between monomers in $2G_2$-*m*-Per is somewhat hindered by the delocalization expected through ortho-substituted segments. In the unsymmetrical dendrons, the ortho substitution is expected to have qualitatively similar characteristics as para substitution, and thus the electron−hole pair is expected to be delocalized within each monodendron. The meta substitution at the core does not allow the exciton delocalization to go beyond the central phenyl group, and the exciton is confined to individual monodendrons.

Once the excitation is created, it can migrate via two pathways (direct or indirect) towards the bottom of the energy funnel. Since both donor and acceptor have allowed optical transitions with strong oscillator strengths, the largest contribution to the coupling will be due to Coulombic interactions. The magnitude of the Coulombic coupling can lead to incoherent exciton migration for weak interactions or coherent exciton transfer for strong interactions.

Energy migration can be interpreted using the simplest model (Förster) that invokes very weak coupling between two point dipoles.[33] The point dipole/point dipole coupling approximation is valid when the donor−acceptor separation (R) is much larger than the dipole sizes. The very weak coupling is valid when the homogeneous vibronic bandwidth is larger than the dipole−dipole coupling. For the dendritic macromolecule under investigation, we evaluate the validity of each of these conditions independently.

The excitation transfer rate in the weak-coupling limit can be calculated from[34]

$$k_{ET} = \frac{4\pi^2}{h^2 c} J|U|^2 \quad (9)$$

where U is the coupling and J is the vibronic spectral overlap integral (in units of cm) between donor and acceptor. The spectral overlap is a measure of the density of interacting initial and final states. The accurate calculation of the overlap integral employs the homogeneous vibronic bandwidths. Since the homogeneous bandwidths of the vibronic bands in the didendron are unknown, we rely on absorption and emission spectra to obtain J. The spectral density can be evaluated by using a normalized absorption spectrum acceptor, $A(\lambda)$, and normalized emission spectra donor, $F(\lambda)$

$$J(\mathrm{cm}) = \int_{\lambda_i}^{\lambda_f} A(\lambda)F(\lambda)\lambda^2(\mathrm{nm})10^{-7}\,\mathrm{d}\lambda \qquad (10)$$

yielding $J = 2.02 \times 10^{-4}$ cm.

An experimentally measured transfer rate $k_{ET} = (750\ \mathrm{fs})^{-1}$ yields an interaction energy $U = 75\ \mathrm{cm}^{-1}$. The approximation in the J calculation results in an upper limit for J and therefore, for a given experimental rate, a lower limit for the Coulombic interaction.

Donor and acceptor spectra in the 350−450 nm (28 600−22 200 cm^{-1}) range are very broad. Measuring single-molecule fluorescence, Schryver and co-workers[35] estimated vibronic bandwidths between 650 and 850 cm^{-1}. Even though this number might be an overestimation of the true homogeneous bandwidth, it is still very large compared to the small Coulombic interaction energy, endorsing the use of the very weak coupling model.

To understand the role of the dipole size, we again assume the Förster model and compare the result of this model with the experimental values. The critical radius R_0 (the distance at which emission and energy transfer occur with equal probability) for the energy-transfer step between monodendron excited state E* and phenyl ethynylene perylene excited state P* can be evaluated from

$$R_0 = 0.2108\left[\frac{\kappa^2\Phi_D}{n^4}\int_0^\infty I_D(\lambda)\epsilon_A(\lambda)\lambda^4\,\mathrm{d}\lambda\right]^{1/6} \qquad (11)$$

where κ^2 is the orientation factor ($\kappa^2_{avg} = {}^2/_3$), Φ_D is the fluorescence quantum yield of the donor in the absence of the acceptor, n is the index of refraction of the solvent (1.4 for CH_2Cl_2), $I_D(\lambda)$ is the normalized fluorescence spectrum, and $\epsilon_A(\lambda)$ is the molar extinction coefficient of the acceptor. The overlap integral (in units of cm^6/mol) is evaluated by taking the normalized emission spectrum of $2G_2$-*m*-OH and the absorption extinction coefficient of phenyl ethynylene perylene. With these parameter values, we find $R_0 = 44.25$ Å.

Molecular dynamic simulations[25] on these macromolecules provide information about the 3D architecture of the didendrons (Scheme 1c). Despite what a 2D chemical structure sketch might suggest, the unsymmetrical dendrimers are not planar. The 3D conformation has a somewhat rigid Y shape with only the peripheral phenyl groups rotating almost freely around the ethynylene bonds. These MD simulations[25] allow the evaluation of the moieties' sizes, yielding ∼15.5 Å for the monodendron and ∼13.5 Å for the phenyl ethynylene perylene. The distance between the center of each monodendron to the center of the phenyl ethynylene perylene unit is ∼17.2 Å. If we consider that the monodendrons size will be on the order of the dipole size, then we would expect an energy-transfer rate constant of $(6.5\ \mathrm{ps})^{-1}$. Experimentally, the energy-transfer rate constant is $(750\ \mathrm{fs})^{-1}$, clearly indicating that the Förster model cannot account for this fast process. The disparity in the calculated versus measured rates is due to the sizes of the chromophores, which are very similar to the dipole−dipole distances and to the assumption that in a point dipole description the dipole is located at the "spatial" center of each dendron. A point dipole approximation does not account for the transition dipole density distribution, which becomes an important factor when dipoles are in close proximity.[15]

A better treatment of the Coulombic coupling must include at least the transition dipole shape and distribution and can be performed using the transition density cube method,[16,36] which provides a numerical approximation to the complete Coulombic coupling.

Conclusions

We measured the fluorescence dynamics of a phenyl ethynylene didendron with and without an energy trap. The fast transfer dynamics yield a highly efficient light-harvester, with a sub-picosecond time scale for energy transfer.

On the basis of steady-state spectroscopy, initial studies of unsymmetrical architectures suggested that the electronic structure could be interpreted as the addition of individual building blocks. The time-resolved data presented in this work suggest that the building blocks encompass each monodendron, with two possible pathways for exciton migration. The presence of a combination of ortho and para substitution leads to initial exciton delocalization within each monodendron, and the meta substitutions confine them there. The electronic structures of the monodendron and the trap are weakly coupled, though a more complete characterization of dipole size and shape is required to accurately simulate the transfer rates.

Linear symmetric dendrimers with phenyl ethynylene units of variable lengths[10] show energy gradients due to the localization of excitons on the different length PE units. For unsymmetrical dendrimers, the ortho and para substitutions suggest a complete initial delocalization within the monodendrons. In the $2G_2$-*m*-OH system, delocalization is found in the initially excited state (since all results are independent of excitation wavelength). After excitation, a change in the excited-state surface leads to localization and the formation of an energy gradient. This excited-state energy gradient yields efficient multistep energy transfer in the $2G_2$-*m*-Per macromolecule. Roughly 50% of the energy transfer occurs through a multistep pathway, but the process is still completed in a sub-picosecond time scale. It is therefore our suggestion that increasing the generation size will increase the number of absorbing units while maintaining the highly efficient light-harvesting properties.

Acknowledgment. We thank Professor Krause and Professor Roitberg for sharing unpublished MD data with us and Dr. Müller for very fruitful discussions. This work was generously supported by the National Science Foundation (Grant No. CHE-0239120).

References and Notes

(1) Adronov, A.; Frechet, J. M. J. *Chem. Commun.* **2000**, 1701.
(2) Devadoss, C.; Bharathi, P.; Moore, J. S. *J. Am. Chem. Soc.* **1996**, *118*, 9635.
(3) Adronov, A.; Robello, D. R.; Frechet, J. M. J. *J. Polym. Sci., Part A: Polym. Chem.* **2001**, *39*, 1366.
(4) Frechet, J. M. J. *Science* **1994**, *263*, 1710.
(5) Newkome, G. R.; Moorefield, C. N.; Vogtle, F. *Dendrimers and Dendrons: Concepts, Syntheses, Applications*, 2nd ed.; Wiley-VCH: New York, 2001.
(6) Tomalia, D. A.; Naylor, A. M.; Goddard, W. A. *Angew. Chem., Int. Ed. Engl.* **1990**, *29*, 138.
(7) McElhanon, J. R.; McGrath, D. V. *J. Am. Chem. Soc.* **1998**, *120*, 1647.

(8) Balzani, V.; Ceroni, P.; Juris, A.; Venturi, M.; Campagna, S.; Puntoriero, F.; Serroni, S. *Coord. Chem. Rev.* **2001**, *219*, 545.

(9) Gilat, S. L.; Adronov, A.; Frechet, J. M. J. *Angew. Chem., Int. Ed.* **1999**, *38*, 1422.

(10) Shortreed, M. R.; Swallen, S. F.; Shi, Z. Y.; Tan, W. H.; Xu, Z. F.; Devadoss, C.; Moore, J. S.; Kopelman, R. *J. Phys. Chem. B* **1997**, *101*, 6318.

(11) Kopelman, R.; Shortreed, M.; Shi, Z. Y.; Tan, W. H.; Xu, Z. F.; Moore, J. S.; BarHaim, A.; Klafter, J. *Phys. Rev. Lett.* **1997**, *78*, 1239.

(12) Thompson, A. L.; Gaab, K. M.; Xu, J. J.; Bardeen, C. J.; Martinez, T. J. *J. Phys. Chem. A* **2004**, *108*, 671.

(13) Tretiak, S.; Chernyak, V.; Mukamel, S. *J. Phys. Chem. B* **1998**, *102*, 3310.

(14) Minami, T.; Tretiak, S.; Chernyak, V.; Mukamel, S. *J. Lumin.* **2000**, *87*−*9*, 115.

(15) Ortiz, W.; Krueger, B. P.; Kleiman, V. D.; Krause, J. L.; Roitberg, A. E. *J. Phys. Chem. B* **2005**, *109*, 11512.

(16) Ortiz, W.; Roitberg, A. E.; Krause, J. L. *J. Phys. Chem. B* **2004**, *108*, 8218.

(17) Kleiman, V. D.; Melinger, J. S.; McMorrow, D. *J. Phys. Chem. B* **2001**, *105*, 5595.

(18) Ranasinghe, M. I.; Hager, M. W.; Gorman, C. B.; Goodson, T. *J. Phys. Chem. B* **2004**, *108*, 8543.

(19) Swallen, S. F.; Zhu, Z. G.; Moore, J. S.; Kopelman, R. *J. Phys. Chem. B* **2000**, *104*, 3988.

(20) Gaab, K. M.; Thompson, A. L.; Xu, J. J.; Martinez, T. J.; Bardeen, C. J. *J. Am. Chem. Soc.* **2003**, *125*, 9288.

(21) Pan, Y. C.; Lu, M.; Peng, Z. H.; Melinger, J. S. *J. Org. Chem.* **2003**, *68*, 6952.

(22) Pan, Y. C.; Peng, Z. H.; Melinger, J. S. *Tetrahedron* **2003**, *59*, 5495.

(23) Peng, Z. H.; Pan, Y. C.; Xu, B. B.; Zhang, J. H. *J. Am. Chem. Soc.* **2000**, *122*, 6619.

(24) Melinger, J. S.; Pan, Y. C.; Kleiman, V. D.; Peng, Z. H.; Davis, B. L.; McMorrow, D.; Lu, M. *J. Am. Chem. Soc.* **2002**, *124*, 12002.

(25) Roitberg, A. E, Krause, J. L. The system was built in Hyperchem 7.0 and run for 100 ns ($T = 300$ K) using the program Tinker. (Ponder, J. *TINKER, Software Tools for Molecular Design*, version 3.9; Washington University: St. Louis, MO, 2003. The most updated version for the TINKER program can be obtained from J. W. Ponder's website at http://dasher.wustl.edu/tinker.) The MM3 force field was used, with the rotational barrier around the ethynylene triple bond raised to 0.6 kcal/mol to reflect experimental observables. The simulations were performed in a vacuum and should be interpreted only as guides to overall conformational shapes.

(26) Davis, B. L.; Melinger, J. S.; McMorrow, D.; Peng, Z. H.; Pan, C. Y. *J. Lumin.* **2004**, *106*, 301.

(27) Swallen, S. F.; Kopelman, R.; Moore, J. S.; Devadoss, C. *J. Mol. Struct.* **1999**, *486*, 585.

(28) After many hours of UV excitation, we detect some changes in the emission spectrum due to photobleaching. We were careful to change samples before any degradation occurs.

(29) Varnavski, O. P.; Ostrowski, J. C.; Sukhomlinova, L.; Twieg, R. J.; Bazan, G. C.; Goodson, T. *J. Am. Chem. Soc.* **2002**, *124*, 1736.

(30) Varnavski, O.; Menkir, G.; Goodson, T.; Burn, P. L. *Appl. Phys. Lett.* **2000**, *77*, 1120.

(31) Melinger, J. S.; Davis, B. L.; McMorrow, D.; Pan, C. Y.; Peng, Z. H. *J. Fluoresc.* **2004**, *14*, 105.

(32) The purity of the sample was checked by thin layer chromatography (TLC). In addition, we performed an experiment by titrating the 2G2-*m*-Per with 2G2-*m*-OH, comparing absorption and emission spectra as a function of added 2G2-*m*-OH. We conclude that the spectroscopy experiments are more sensitive than TLC and can detect 1−2% impurity. A concentration of 1% 2G2-*m*-OH yields at least 99% of the integrated fluorescence of the band peaked at 435 nm seen in Figure 3.

(33) Förster, T. *Modern Quantum Chemistry*; Academic Press: New York, 1965; Vol. 3.

(34) Valeur, B. *Molecular Fluorescence: Principles and Applications*; Wiley-VCH: Weinheim, Germany, 2002.

(35) Hofkens, J.; Cotlet, M.; Vosch, T.; Tinnefeld, P.; Weston, K. D.; Ego, C.; Grimsdale, A.; Mullen, K.; Beljonne, D.; Bredas, J. L.; Jordens, S.; Schweitzer, G.; Sauer, M.; De Schryver, F. *Proc. Natl. Acad. Sci. U.S.A.* **2003**, *100*, 13146.

(36) Krueger, B. P.; Scholes, G. D.; Jimenez, R.; Fleming, G. R. *J. Phys. Chem. B* **1998**, *102*, 2284.